Quantum Assisted Combinatorial Benders' Algorithm for the Synergy of Hydrogen and Power Distribution Systems with Mobile Storage

Mingze Li, *IEEE Student Member,* Siyuan Wang, *IEEE Senior Member,* Lei Fan, *IEEE Senior Member,* and Zhu Han, *IEEE Fellow*

***Abstract*—The growth of hydrogen infrastructure is expected to aid in the integration of fluctuating renewable energy in distribution systems. To leverage the hydrogen system flexibility, this work presents a mixed-binary quadratic program (MBQP) model for synergistic operations of hydrogen and power distribution systems, wherein truck-mounted mobile hydrogen storage facilities are modeled for the schedule of their routes and loading/unloading quantities. A quantum-assisted combinatorial Benders' decomposition algorithm is designed for our MBQP model to deploy the solving of master and sub-problems on a quantum processing unit (QPU) and a classical CPU, respectively. The master problem is reformulated as a quadratic unconstrained binary optimization (QUBO) problem, which can be efficiently solved by quantum annealers. The proposed approach was tested on a hybrid quantum annealing and classical computing platform. Results show a trend to outperform the CPU-based commercial solvers as the problem scale increases.**

***Index Terms*—Quantum Computing, Combinatorial Benders' Decomposition, Hydrogen, Mobile Hydrogen Storage, Power Distribution System.**

NOMENCLATURE

Indices

b, t, z	Index for buses, time periods and zones

Sets

$\mathcal{B}$	Set of total buses
$\mathcal{B}_{root}$	Set of substation buses
$\mathcal{HE}$	Set of electrolyzors
$\mathcal{HE}_b$	Set of electrolyzors connected with bus b
$\mathcal{HE}_z$	Set of electrolyzors in zone z
$\mathcal{HR}$	Set of steam methane reformers
$\mathcal{HR}_z$	Set of steam methane reformers in zone z
$\mathcal{PV}$	Set of photovoltaic generator systems
$\mathcal{T}$	Set of hourly time periods
$\mathcal{TK}$	Set of trucks
$\mathcal{Z}$	Set of hydrogen zones

Parameters

η_i	Power-to-hydrogen efficiency of electrolyzor i
$\lambda_{b,t}$	Local marginal price (LMP) from the wholesale market received at bus b and time t
$\overline{C}_i$	Loading capacity of mobile hydrogen storage (MHS) i
$\overline{H}_i$	Maximum production of hydrogen producer i
$\overline{E}_z$	Hydrogen mass that can be stored in zone z
$\overline{S}_{i,t}^{PV,p}, \overline{S}_{i,t}^{PV,q}$	Active/Reactive power limit of photovoltaic generation system i
$\underline{V}_b, \overline{V}_b$	Lower/upper limit power of squared voltage magnitude at bus b
c^{fuel}	Cost of transportation
$c_i^{\text{lding}}, c_i^{\text{unlding}}$	Cost of loading/unloading of truck i
c_i^{prd}	Cost of steam methane reformer i
$D_{z,t}^{hyd}$	Hydrogen load in zone z at time t
$d_{z_{st},z_{en}}$	Route length from zone z_{st} to z_{en}
$e_{z,0}$	Hydrogen storage at the initial time period
$e_{z,\|\mathcal{T}\|}$	Hydrogen storage at the last time period
$NTK_{z,t}$	Maximum truck quota in zone z at time t
$p_{b,t}^D$	Active electricity load at bus b and time t
$q_{b,t}^D$	Reactive electricity load at bus b and time t
$r_{m,n}, x_{m,n}$	Resistance, reactance of branch (m,n)
$S_{m,n}$	Maximum power capacity of branch (m,n)

Decision Variables

$e_{i,t}^{\text{mhs}}$	Loading level of MHS i in time t
$f_{m,n,t}^P, f_{m,n,t}^Q$	Active/reactive flow from bus m to n at time t
$h_{i,t}$	Hydrogen generation of steam methane reformer i at time t
$p_{b,t}^{root}, q_{b,t}^{root}$	Active/Reactive power generation of bus b at time t
$p_{i,t}^{HE}, q_{i,t}^{HE}$	Active/Reactive power consumption of electrolyzor i at time t
$p_{i,t}^{PV}, q_{i,t}^{PV}$	Active/Reactive power generation of solar station i at time t
$q_{i,z,t}^{\text{lding}}, q_{i,t}^{\text{unlding}}$	Loading/Unloading hydrogen quantity of MHS i in site z and time t
$u_{b,t}$	Power rate of bus b at time t
$x_{i,z,t}$	Binary variable indicating if MHS i is in zone z at the end of time t, 1 indicates that MHS i is in zone z

This work was supported by National Science Foundation (NSF) under Grants CNS-2107216, CNS-2128368, CMMI-2222810, ECCS-2302469, ECCS-2045978. (Corresponding Author: Lei Fan.)

Mingze Li is with the Department of Electrical and Computer Engineering, and the Department of Engineering Technology, University of Houston, Houston, TX 77204 USA (e-mail: mli44@cougarnet.uh.edu)

Siyuan Wang is with the Energy Systems and Infrastructure Analysis Division, Argonne National Laboratory, Lemont, IL 60439, USA (e-mail: siyuan.wang@anl.gov)

Lei Fan is with the Department of Engineering Technology, and the Department of Electrical and Computer Engineering, University of Houston, Houston, TX 77204 USA (e-mail: lfan8@central.uh.edu).

Zhu Han is with the Department of Electrical and Computer Engineering at the University of Houston, Houston, TX 77004 USA, and also with the Department of Computer Science and Engineering, Kyung Hee University, Seoul, South Korea, 446-701 (e-mail: zhan2@uh.edu).

I. Introduction

THE integration of renewable energy sources into power distribution systems presents a significant challenge due to the fluctuating nature of these resources. A series of studies are proposed to analysis and utilize renewable power recently [1]. Hydrogen networks can potentially offer flexibility for power systems to address the aforementioned issue because they have relatively low needs for real-time energy balancing. Leveraging this feature eventually requires mathematical models for the two systems' synergistic operations, and advanced solution approaches to tackle the expected model size increase in the future.

This growing interest in hydrogen as an intermediary for excess renewable energy emphasizes the need to develop robust strategies that optimize the integration of these two critical sectors. Flexibly converting surplus renewable energy to hydrogen meanwhile considering the storage capabilities in the hydrogen system is urgently needed to investigate. Recent studies have started to explore the interaction between power and hydrogen sectors from various point of views. For station level systems, a hydrogen filling station for fuel cell vehicles is designed in [2]. The authors of [3] present a control strategy for a stand-alone hybrid renewable energy and hydrogen storage system. There has been some researchers who utilize microgrid to achieve energy management [4]. For microgrid or local multi-energy systems, [5] presents an operation strategy for a microgrid with renewable energy and a power-to-hydrogen scheme. In [6], a deep deterministic policy gradient based hybrid energy scheduling (H-DDPG) algorithm is proposed to convert surplus renewable energy into hydrogen through electrolysis. A hydrogen-based networked microgrids planning approach is proposed in [7] in the presence of renewable energy sources by using two-stage stochastic programming with mixed-integer conic recourse. The utilization of hydrogen in local energy systems for internet data centers is explored in [8]. From a bulk power system perspective, [9] investigated how power-hydrogen interactions can affect power transmission expansion planning, with modeling of hydrogen transportation networks and centralized hydrogen storage. A generation capacity expansion is proposed in [10] considering further considerations of H2-fired gas turbines and energy storage systems. For power distribution systems, a simplified power-to-hydrogen dispatch model is proposed for the electricity-heat-hydrogen dispatch coordinated with active distribution networks and district heating networks [11]. This growing need to optimize the integration of hydrogen and power systems is underscored by recent studies investigating hydrogen storage's roles within these networks [12]. Moreover, developing risk-constrained bidding strategies for integrated electricity-hydrogen energy systems is crucial to enhance their economic viability in competitive markets [13]. Our recent work [14] further presents a coordinated operation approach of hydrogen and power distribution systems considering pipeline hydrogen transportation systems. Pipeline would be economic when the demand is relatively large in a future scenario. For most current cases, truck-mounted mobile hydrogen storage is a more viable way, the roles of which are worth further investigation.

These works have explored various aspects of the interaction between power and hydrogen systems, but in the context of power distribution systems, how electrolysis and mobile hydrogen storage resources benefit hydrogen and power synergistic operations can be explored under near-future scenarios. The routine scheduling of truck-mounted mobile hydrogen storage facilities needs a detailed consideration. We also aim to maximize the utilization of renewable generation with flexible synergistic dispatch. When the electricity price from the wholesale market is low or the power from a renewable power station is sufficient, the coordinated system can convert the surplus energy to hydrogen and transport them via the truck-mounted mobile hydrogen storage system. Considering these above facts, we model the synergistic operation as a mixed-binary quadratic program (MBQP), wherein individual-level route and loading/unloading scheduling of truck-mounted mobile hydrogen storage facilities are modeled with more realistic path-dependent travel costs.

To tackle the complex MBQP problem, the Benders' decomposition algorithm [15] is recognized as an efficient way to solve the proposed mixed-binary programs. The rapid development of quantum computing offers promising features that can potentially outperform algorithms on classical computers. Quantum computing is also showing its potential in the energy domain [16], [17]. However, the hardware limit of current quantum processing unit (QPU) hinders the validation through scalability testing. To tackle this, we propose a quantum-assisted combinatorial Benders' decomposition approach that can benefit from both classical and quantum computing capabilities. Comparing to Benders' decomposition deployment on pure CPU, trends of performance improvements can be more visible with slightly larger-scale instances enabled by our hybrid approach. Generally, the development of quantum computing techniques can be categorized into two directions: gate-based quantum computers and quantum annealers. Currently, the gate-based quantum computer is limited to less than 100 quantum bits [18]. D-Wave Systems Inc., on the other hand, manufactures quantum annealers with 5,000 quantum bits (qubits). A quantum annealer has just been verified for its strong computation ability to solve binary optimization problems [19]. The quantum annealing algorithm can only be used to solve quadratic unconstrained binary optimization (QUBO) at present. Some problems can be modeled using QUBO and solved by a quantum annealer directly [20], [21]. However, our problem is a MBQP model and need to be reformulated to QUBO.

With Benders' decomposition, the MBQP model for synergistic operation is separated to mixed-binary nonlinear master problems and linear sub problems, which are deployed in quantum and classical computers, respectively. The mixed-binary nonlinear master problem is reformulated as a QUBO, which can be solved by quantum annealers. Note although various previous works have converted mixed-binary linear programs (MBLPs) to QUBOs and applied to practical problems [22], our approach addresses a specific MBQP for synergistic operations of hydrogen and power distribution systems. Furthermore, our QUBO reformulation approach can

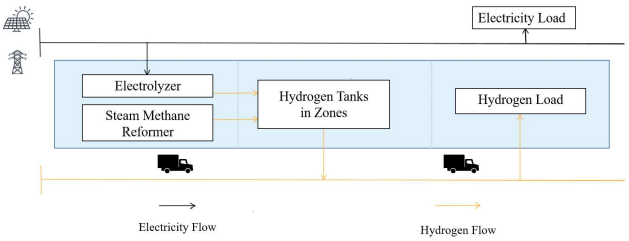

Fig. 1. The framework of synergistic operation

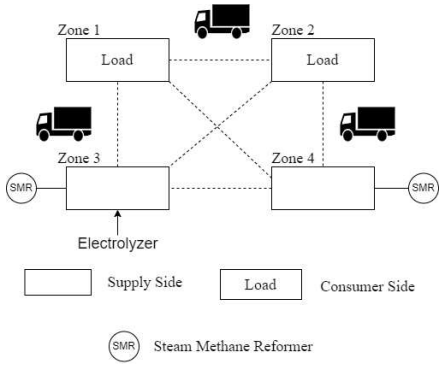

Fig. 2. The framework of hydrogen system

be generically extended to addressing a class of MBQPs. There has been studies to utilize quantum machines to solve Benders' decomposition problems recently [23].

The contributions of this work are summarized in the following.

- A MBQP model is proposed for synergistic operations of hydrogen and power distribution systems, in which truck-mounted mobile hydrogen storage facilities are modeled in individual level to schedule their routes and loading/unloading quantities.
- A tailored quantum assisted combinatorial quantum Benders' decomposition algorithm is designed to solve the MBQP model. The resulting mixed-binary quadratic master problems and linear subproblems are solved on quantum and conventional computers, respectively.
- In comparison to classical computer based Benders' decomposition, our hybrid quantum approach shows a trend to be more scalable, especially in solving nonlinear master problems with a fair number of cuts added.

II. MBQP Model for Synergistic Operations with Truck-mounted Hydrogen Storage

In this section, we describe a mathematical programming model for the synergistic operations for power distribution system and the hydrogen system. Then the hydrogen can be produced by electrolyzers with electricity.

A. Objective Function

The objective function is defined as the sum of the operation costs for hydrogen production, transportation, and power distribution systems.

$$\min \ \varphi = C^{\mathrm{h2prd}} + C^{\mathrm{h2trs}} + C^{\mathrm{ele}}. \tag{1}$$

We denote the cost of hydrogen production by C^{h2prd}. The cost of each steam methane reformer is represented by c_i^{prd}, which is assumed a constant value. The amount of hydrogen production of steam methane reformer i at time period t is defined as $h_{i,t}$.

$$C^{\mathrm{h2prd}} = \sum_{t\in\mathcal{T}} \sum_{i\in\mathcal{HR}} c_i^{\mathrm{prd}} \cdot h_{i,t}. \tag{2}$$

We also use C^{h2trs} to model the hydrogen transportation cost. The loading and unloading cost is modeled as a linear function and the fuel cost for traveling is modeled as a quadratic function of distance. Our model operates on an hourly time scale, meaning that it is designed to simulate and optimize hydrogen production, transportation, and energy usage in hourly increments. Given the current limitations in the computational power of quantum computers, we have constrained the model to focus on transportation within a small geographical area, such as an urban region. This allows for the assumption that a truck can transport hydrogen or goods from one area to another within one hour, reducing the overall complexity of the problem and making it more manageable with the available quantum computing resources. Therefore, only when $x_{i,z_{st},t-1}$ and $x_{i,z_{en},t}$ are both equal to 1, the fuel cost is added to the objective function; otherwise, it will be zero.

$$C^{\mathrm{h2trs}} = \sum_{t\in\mathcal{T}} \sum_{z\in\mathcal{Z}} \sum_{i\in\mathcal{TK}} (c_i^{\mathrm{lding}} \cdot q_{i,z,t}^{\mathrm{lding}} + c_i^{\mathrm{unlding}} \cdot q_{i,z,t}^{\mathrm{unlding}}) + \sum_{t\in\mathcal{T}} \sum_{i\in\mathcal{TK}} \sum_{z_{st}\in\mathcal{Z}} \sum_{z_{en}\in\mathcal{Z}} c^{\mathrm{fuel}} \cdot d_{z_{st},z_{en}} \cdot x_{i,z_{en},t} \cdot x_{i,z_{st},t-1}. \tag{3}$$

Next, $\mathcal{B}_{root}$ contains substation bus(es). $\hat{\lambda}_{b,t}$ is the local marginal price (LMP) from the wholesale electricity market, while $p_{b,t}^{root}$ is the power generation from each substation bus at time t. Then, the electricity cost from the wholesale electricity market can be described as,

$$C^{\mathrm{ele}} = \sum_{t\in\mathcal{T}} \sum_{b\in\mathcal{B}_{root}} \hat{\lambda}_{b,t} \cdot p_{b,t}^{root}. \tag{4}$$

B. Hydrogen Distribution System Constraints

The hydrogen production and truck-mounted mobile hydrogen storage facilities are modeled in this section. Fig. 2 shows the framework of hydrogen distribution system. There are 2 steam methane reformers in Zones 3 and 4, which can produce hydrogen to meet the loads in Zones 1 and 2. The hydrogen is transported from the producer side to the consumer side by trucks. There are routines between the two zones. An extra electrolyzor can be added to Zone 3 to transform extra electricity to hydrogen from power distribution system. The modeling of the hydrogen system is shown below.

1) Hydrogen Production: The hydrogen production of steam methane reformers and electrolyzors cannot exceed the

upper bound $\overline{H}_i$ in each time period. Then the bounds for two types of hydrogen production units are shown as,

$$0 \le h_{i,t} \le \overline{H}_i \quad \forall i \in \mathcal{HR}, t \in \mathcal{T}, \tag{5a}$$

$$0 \le \eta_i \cdot p^{HE}_{i,t} \le \overline{H}_i \quad \forall i \in \mathcal{HE}, t \in \mathcal{T}. \tag{5b}$$

2) Hydrogen Mass Balance: The constraints represent the balance at the zonal level as,

$$0 \le e_{z,0} + \sum_{\tau=1}^{t} \left(\sum_{i \in \mathcal{HR}_z} h_{i,\tau} + \sum_{i \in \mathcal{HE}_z} \eta_i \cdot p^{HE}_{i,\tau} - \sum_{i \in \mathcal{TK}} q^{\text{lding}}_{i,z,\tau} + \sum_{i \in \mathcal{TK}} q^{\text{unlding}}_{i,z,\tau} - D^{\text{hyd}}_{z,\tau} \right) \le \overline{E}_z, \forall z \in \mathcal{Z}, t \in \mathcal{T} \backslash \{|\mathcal{T}|\}. \tag{6a}$$

$$e_{z,0} + \sum_{\tau \in \mathcal{T}} \left(\sum_{i \in \mathcal{HR}_z} h_{i,\tau} + \sum_{i \in \mathcal{HE}_z} \eta_i \cdot p^{HE}_{i,\tau} - \sum_{i \in \mathcal{TK}} q^{\text{lding}}_{i,z,\tau} + \sum_{i \in \mathcal{TK}} q^{\text{unlding}}_{i,z,\tau} - D^{\text{hyd}}_{z,\tau} \right) = e_{z,|\mathcal{T}|}, \forall z \in \mathcal{Z}, \tag{6b}$$

where the level of hydrogen mass in each time period is determined by the input and output of hydrogen. This includes hydrogen production through steam methane reformers and electrolyzers, as well as hydrogen loads and the amount of hydrogen loaded and unloaded by trucks. (6a) limits that the hydrogen mass cannot exceed the capacity that can be stored. (6b) defines the hydrogen mass level at the end of time horizon.

3) Mobile Hydrogen Storage: Here we have an assumption that vehicles can travel from one zone to any other zone in one interval, and fuel cost for traveling is modeled as a quadratic function of distance. The upper bound limits for loading and unloading amount for each truck in each zone are modeled in (7a) and (7b), respectively. Constraints (7c) represent each truck can only be in one zone in each period. (7d) limited the maximum number of trucks for a zone at each time period. Constraints (7e) and (7f) represent the tank storage dynamics and their state of charge limits.

$$0 \le q^{\text{lding}}_{i,z,t} \le \overline{C}_i \cdot x_{i,z,t}, \forall i \in \mathcal{TK}, \forall z \in \mathcal{Z}, t \in \mathcal{T}, \tag{7a}$$

$$0 \le q^{\text{unlding}}_{i,z,t} \le \overline{C}_i \cdot x_{i,z,t}, \forall i \in \mathcal{TK}, \forall z \in \mathcal{Z}, t \in \mathcal{T}, \tag{7b}$$

$$\sum_{z \in \mathcal{Z}} x_{i,z,t} = 1, \forall i \in \mathcal{TK}, t \in \mathcal{T}, \tag{7c}$$

$$\sum_{i \in \mathcal{TK}} x_{i,z,t} \le NTK_{z,t}, \forall z \in \mathcal{Z}, t \in \mathcal{T}, \tag{7d}$$

$$e^{\text{mhs}}_{i,t+1} = e^{\text{mhs}}_{i,t} + \sum_{z \in \mathcal{Z}} q^{\text{lding}}_{i,z,t} - \sum_{z \in \mathcal{Z}} q^{\text{unlding}}_{i,z,t}, \forall i \in \mathcal{TK}, t \in \mathcal{T}, \tag{7e}$$

$$0 \le e^{\text{mhs}}_{i,t} \le \overline{C}_i, \forall i \in \mathcal{TK}, t \in \mathcal{T}. \tag{7f}$$

C. Power Distribution System Constraints

The physical characteristics of electricity delivery, renewable energy generation, and electrolysis are modeled in this subsection.

1) Power Balance: We model power flow balance for active and reactive power in (8a) and (8b), respectively. Here, if bus b is a substation bus, $1_{b \in \mathcal{B}_{root}} = 1$; otherwise, $1_{b \in \mathcal{B}_{root}} = 0$. Constraint (8c) is added to limit the power flow to zero in disconnected branches. Constraints (8c) and (8d) represents the active and reactive power from solar generation systems are less than their limits.

$$\sum_{(b,n) \in \mathcal{L}} f^P_{b,n,t} - \sum_{(m,b) \in \mathcal{L}} f^P_{m,b,t} = 1_{b \in \mathcal{B}_{root}} \cdot p^{root}_{b,t} + \sum_{i \in \mathcal{W}^b} p^{PV}_{i,t} - \sum_{i \in \mathcal{HE}_b} p^{HE}_{i,t} - p^D_{b,t}, \ \forall b \in \mathcal{B}, \forall t \in \mathcal{T}, \tag{8a}$$

$$\sum_{(b,n) \in \mathcal{L}} f^Q_{b,n,t} - \sum_{(m,b) \in \mathcal{L}} f^Q_{m,b,t} = 1_{b \in \mathcal{B}_{root}} \cdot q^{root}_{b,t} + \sum_{i \in \mathcal{W}^b} q^{PV}_{i,t} - \sum_{i \in \mathcal{HE}_b} q^{HE}_{i,t} - q^D_{b,t}, \ \forall b \in \mathcal{B}, \forall t \in \mathcal{T}, \tag{8b}$$

$$p^{PV}_{i,t} \le \overline{S}^{PV,p}_{i,t} \ \forall i \in \mathcal{PV}, \forall t \in \mathcal{T}, \tag{8c}$$

$$q^{PV}_{i,t} \le \overline{S}^{PV,q}_{i,t} \ \forall i \in \mathcal{PV}, \forall t \in \mathcal{T}. \tag{8d}$$

2) Branch Flow and Voltage Limits: We model the power flow and voltage limits as,

$$u_{m,t} - u_{n,t} = 2\left(r_{m,n} \cdot f^P_{m,n,t} + x_{m,n} \cdot f^Q_{m,n,t}\right), \quad \forall (m,n) \in \mathcal{L}, \forall t \in \mathcal{T}, \tag{9a}$$

$$f^{P\ 2}_{m,n,t} + f^{Q\ 2}_{m,n,t} \le S^2_{m,n}, \quad \forall (m,n) \in \mathcal{L}, \forall t \in \mathcal{T}, \tag{9b}$$

$$\underline{V}^2_b \le u_{b,t} \le \overline{V}^2_b, \quad \forall b \in \mathcal{B}, \forall t \in \mathcal{T}. \tag{9c}$$

Constraints (9a) represent the power flow between m and n. Constraints (9b) constraint the power flow limits. Constraints (9c) represent the voltage magnitude limits.

Power flow limit constraints in (9b) can be linearized with n_k linear constraints as,

$$\phi^k_{m,n} f^P_{m,n,t} + \chi^k_{m,n} f^Q_{m,n,t} \le \psi^k_{m,n}, \quad \forall (m,n) \in \mathcal{L}, \forall t \in \mathcal{T}, \forall k = 1, .., n_k, \tag{10}$$

where $\phi^k_{m,n} = \cos(2k\pi/n_k)$, $\chi^k_{m,n} = \sin(2k\pi/n_k)$, and $\psi^k_{m,n} = S_{m,n} \cdot \cos(\pi/n_k)$.

D. Discussion on Possible Model Extensions

Although our zones are within a one-hour distance, here we discuss the possibility of expanding the model to account for delays, which allows us to handle scenarios where transportation times exceed this simple assumption. In such cases, we introduce a new group of binary variables, $x_{i,z_0,t}$, where i represents the truck, z_0 represents the truck is on its way, and t represents the time period. These variables are essential for tracking whether truck i is en route at time t.

By incorporating these binary variables in (7c), the model can effectively capture the state of the trucks over time. Specifically, when $x_{i,z_0,t} = 1$, it indicates that truck i is on its way at time t. Conversely, when $x_{i,z_0,t} = 0$, the truck is either loading, unloading, or has already completed its trip. This prevents redundant distance calculations for trucks that are already in transit, as their movement is now defined through

the binary variables. To encourage the mobility of MHS, we replace the constraint (3) to:

$$C^{\text{h2trs}} = \sum_{t\in\mathcal{T}}\sum_{z\in\mathcal{Z}}\sum_{i\in\mathcal{TK}}(c_i^{\text{lding}}\cdot q_{i,z,t}^{\text{lding}} + c_i^{\text{unlding}}\cdot q_{i,z,t}^{\text{unlding}}) + \sum_{t\in\mathcal{T}}\sum_{T=1}^{\hat{T}}\sum_{i\in\mathcal{TK}}\sum_{z_{st}\in\mathcal{Z}}\sum_{z_{en}\in\mathcal{Z}} c^{\text{fuel}}\cdot d_{z_{st},z_{en}}\cdot x_{i,z_{en},t}\cdot x_{i,z_{st},t-T}, \tag{11}$$

where $\hat{T}$ is the maximum transportation time.

Moreover, this approach allows the model to account for variable travel times, such as traffic or operational slowdowns, by adjusting the relevant constraints on the binary variables. For example, if we need at least k hours to travel from z_1 to z_2, then we have:

$$x_{i,z_1,t} + x_{i,z_2,t+T} \le 1,\ \forall T \in 1,2,...,k-1, i \in \mathcal{TK}. \tag{12}$$

Further capturing the trucks' movements in time dependent transitions, transportation models can be more flexible, scalable, and capable of addressing more realistic scenarios where travel times are not fixed but influenced by external factors in the future. This can not only avoid redundancy but also ensure the model's computational efficiency while accurately reflecting the dynamic nature of transportation delays.

III. Quantum Assisted Combinatorial Benders' Decomposition

As our model is a mixed-binary quadratic model, it is difficult to solve directly by a classical solver. In this section, we split the variables in a mixed binary program into a mixed binary subproblem and a pure binary quadratic master problem. Then we transform the master problem to a QUBO problem and solve it by quantum annealing.

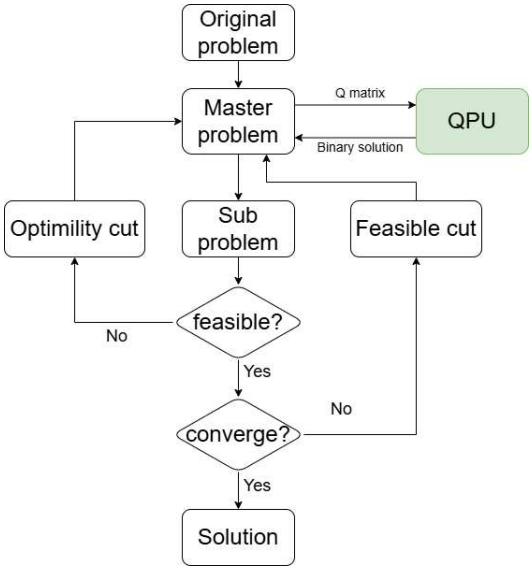

Fig. 3. Flow Chart of Benders' Decomposition

The Quantum Benders' Decomposition process begins by breaking down the original problem into a master problem and a sub problem. The master problem generates an initial solution, which is then passed to the subproblem to check its feasibility. In this flow, the subproblem assesses whether the proposed solution is feasible. If the solution is infeasible, an infeasible cut is added to the master problem, and the process repeats. If the solution is feasible, the subproblem checks for convergence. If the convergence criterion is not met, a feasible cut is added, and the master problem is solved again. In the context of quantum computing, quantum annealer can be used to solve the master problem by transforming it into a quadratic unconstrained binary optimization (QUBO) form, utilizing the Q matrix to get a binary solution. This iterative process continues, alternating between the master problem and subproblem until convergence is achieved, at which point a final solution is found.

A. Quantum Assisted Benders' Decomposition

The proposed synergistic operations model in Section II is a large-scale mixed integer quadratic programming model as

$$\text{OP: } \min_{\mathbf{x},\mathbf{y}} \mathbf{x}^\top U_1^\top \mathbf{x} + \mathbf{y}^\top U_2^\top \mathbf{y} + c^\top \mathbf{x} + d^\top \mathbf{y} + h^\top \mathbf{z}, \tag{13a}$$

$$\text{s.t. } G_1\mathbf{z} \ge b_1, \tag{13b}$$

$$G_2\mathbf{z} = b_2, \tag{13c}$$

$$A_1\mathbf{x} \le b_3, \tag{13d}$$

$$A_2\mathbf{x} = b_4, \tag{13e}$$

$$A_3\mathbf{x} + G_3\mathbf{z} \ge b_5, \tag{13f}$$

$$A_4\mathbf{y} \le b_6, \tag{13g}$$

$$A_5\mathbf{y} = b_7, \tag{13h}$$

$$A_6\mathbf{y} + G_4\mathbf{z} \ge b_8, \tag{13i}$$

$$x \in \mathbf{x},\ x \in \{0,1\}, \tag{13j}$$

$$y \in \mathbf{y},\ y \in \{0,1\}, \tag{13k}$$

$$z \in \mathbf{z},\ z \ge 0. \tag{13l}$$

Here x is a vector with binary variables and U is its nonlinear corresponding coefficient matrix in the objective function, c is the corresponding coefficient vector for linear functions in the objective function, and A is its coefficient matrix in constraints. y is a vector with non-negative continuous variables, where

$$y = \{f^P, f^Q, p^{root}, q^{root}, p^{HE}, q^{HE}, p^W, q^W, u, h, q^{\text{lding}}, q^{\text{unlding}}, e^{\text{mhs}}\} \tag{14}$$

and G is its corresponding coefficient matrix in constraints. $h^\top$ is the coefficient vector of variable y in the objective function. Objective (13a) represents the function (1); constraint (13b) represents constraints (8c), (8d), (9c), (10), (5a)-(6a) and (7f); constraint (13c) represents constraints (8a), (8b), (9a), (6b), (7e); constraint (13d) and (13g) represents (7d); constraint (13e) and constraint (13h) represents (7c); constraint (13f) and constraint (13i) represents (7a) and (7b).

To tackle such a complex model, we proposed a quantum assisted combinatorial Benders' decomposition approach. This approach will divide the original problem into a binary master problem and a subproblem. The binary master problem is a linear constrained quadratic binary programming model, which

can be solved by the quantum anneal algorithm. The subproblem can be solved independently, and the solutions can then be combined to obtain a solution to the original problem. This decomposition technique is particularly effective for problems that have a special structure, such as linear programs with a large number of constraints.

Combinatorial Benders' decomposition emerges as a pivotal strategy for optimizing the use of scarce qubits in quantum computing, specifically tailored for mixed integer programming (MIP) problems. This technique cleverly minimizes the number of binary variables within the master problem. Such a reduction is crucial given the premium on qubits, enabling more efficient allocation and utilization of these limited quantum resources. By strategically lowering the binary variable count in the master problem, the approach compensates for the qubit scarcity by potentially making the integer subproblem more complex. However, this trade-off is worthwhile, as it directly addresses the bottleneck of limited qubit availability, ensuring that computational tasks are more manageable and aligned with the quantum hardware's capacity.

In Problem [OP], where $\mathbf{x}$ and $\mathbf{z}$ represents a set of binary variables and y encapsulates a mixture of continuous and additional binary variables, combinatorial Benders' decomposition diverges from the traditional Benders' decomposition approach. Unlike the classical method, where the subproblems are solved as linear programs, the combinatorial variant retains a portion of the binary variables within the subproblem. This adjustment transforms the subproblem into a mixed binary programming (MBP) challenge. When the binary variables, denoted as $\bar{x}$, are held constant, the formulation gives rise to a specific subproblem, [SP]. This nuanced approach adapts to the complex nature of the variables involved, leading to a strategic partitioning of the problem that accommodates both discrete and continuous decision elements. We denote the subproblem [SP] as:

$$\begin{aligned}
\text{SP: } \theta(\overline{\mathbf{x}}) = \min\ & \mathbf{y}^\top U_2^\top \mathbf{y} + h^T \mathbf{z} \\
\text{s.t. } & G_1\mathbf{z} \geq b_1, \\
& G_2\mathbf{z} = b_2, \\
& G_3\mathbf{z} \geq b_5 - A_3\overline{x}, \\
& A_4\mathbf{y} \leq b_6, \\
& A_5\mathbf{y} = b_7, \\
& A_6\mathbf{y} + G_4\mathbf{z} \geq b_8, \\
& y_j \in \{0,1\} \quad \forall j \in \mathbf{y}, \\
& z_j \geq 0 \quad \forall j \in \mathbf{z},
\end{aligned} \tag{15}$$

and the master problem

$$\begin{aligned}
\text{MP: } \min\ & \mathbf{x}^\top U^\top \mathbf{x} + c^T\mathbf{x} + \theta(\mathbf{x}) \\
\text{s.t. } & A_1\mathbf{x} = b_3, \\
& A_2\mathbf{x} \leq b_4 \\
& x_i \in \{0,1\}.
\end{aligned} \tag{16}$$

According to [24], if a solution x^v of [MP] leads to an infeasible [SP], then x^v is infeasible for problem [OP]. Thus at least one component of x^v should be changed to make [SP] feasible. This is formulated as a feasibility cut

$$\sum_{i:x_i^v=0} x_i + \sum_{i:x_i^v=1} (1-x_i) \geq 1, \tag{17}$$

which is appended to problem [MP]. The feasibility cut (17) is identical to the combinatorial Benders' cuts presented in [24]. If problem [SP] is feasible, with an optimal objective value $\theta^v = h^T y^v$, then the optimal solution of problem [OP] is the best objective function value of problem [MP]. In that case, an optimality cut

$$M^v \sum_{i:x_i^v=0} x_i + M^v \sum_{i:x_i^v=1} (1-x_i) + \theta \geq h^T y^v, \tag{18}$$

is generated and appended to problem [MP]. M^v is a big-M parameter that would make constraint (18) only active for $x = x^v$. Hence, the updated master problem is as follows:

$$\begin{aligned}
\text{FMP: } \min_{\mathbf{x}}\ & \mathbf{x}^\top U^\top \mathbf{x} + c^T\mathbf{x} + \theta && \text{(19a)} \\
\text{s.t. } & \sum_{z\in\mathcal{Z}} x_{i,z,t} = 1, \forall i \in \mathcal{TK}, t \in \mathcal{T}, && \text{(19b)} \\
& \sum_{i\in\mathcal{TK}} x_{i,z,t} \leq NTK_{z,t}, \forall z \in \mathcal{Z}, t \in \mathcal{T}, && \text{(19c)} \\
& M^v \sum_{i:x_i^v=0} x_i + M^v \sum_{i:x_i^v=1} (1-x_i) + \theta \geq d^T y^v \\
& \forall v \in V^{\mathrm{P}}, && \text{(19d)} \\
& \sum_{i:x_i^v=0} x_i + \sum_{i:x_i^v=1} (1-x_i) \geq 1, \quad \forall v \in V^{\mathrm{R}}, && \text{(19e)} \\
& x \in \mathbf{x}, x \in \{0,1\}^n. && \text{(19f)}
\end{aligned}$$

The sets of the extreme points and the extreme rays of the feasible region of subproplem, are denoted by V^{P} and V^{R}, respectively. Master problem [MP] is a relaxation of original problem [OP] when subsets of V^{P} and V^{R} are present. Therefore, solving [MP] yields a lower bound (LB) on the optimal solution of problem [OP]. Similar to the classical Benders' decomposition algorithm, the upper and lower bounds are used as a stopping criteria for the cutting plane algorithm.

Overall, Benders' decomposition is a powerful tool for solving large-scale optimization problems. However, though the master problem is simplified, it is still difficult to solve when the problem size is large. Thus, in the next section, we transform the master problem to a QUBO problem and utilize the advantage of quantum annealer to solve it.

B. QUBO Model

Quantum annealing (QA) provides a new method to solve QUBO problems. Some researchers have been proposed to utilize QA [25]. To solve this problem efficiently, we further reformulate problem [FMP] to a QUBO problem, which can be solved by quantum annealing.

In recent years, quantum annealer has been developed as a new and effective approach to solve a QUBO problem. A quantum annealer can be used to solve discrete optimization problems with specific structures because it tends to retain lowest energy state. If a problem can be expressed as the

energy states of a system, it can be fed to quantum annealers to solve. The QPU of a quantum annealer, which functions like the CPU in a classical computer, is made up of connected qubits that create a graph topology. This creates a physical system whose energy is measured by a function of its states called the Hamiltonian [26]. An arbitrary QUBO problem can be expressed by a Hamiltonian function:

$$f = \sum_{i=0}^{N-2} \sum_{j=i+1}^{N-1} J_{i,j} \sigma_i^Z \sigma_j^Z + \sum_{i=0}^{N-1} h_i \sigma_i^Z. \tag{20}$$

The Pauli-z matrix, denoted as σ_i^Z, acts on qubit i and has eigenvalues of ± 1. The coefficient $J_{i,j}$ determines the relationship between σ_i^Z and σ_j^Z, which corresponds to the entanglement part of the model. On the other hand, h_i corresponds to the individual part. While $x_i \in \{0, 1\}$ and $\sigma_i^Z \in \{+1, -1\}$, x_i is reformulated as $\left(1 - \sigma_i^Z\right)/2$. Hence, solving the QUBO problem is to finding a binary vector $\mathbf{x}^*$ that minimizes f by converting the variables x_i to σ_i^Z, i.e.,

$$\mathbf{x}^* = \arg\min_{\mathbf{x}} \ f(\mathbf{x}). \tag{21}$$

Now consider problem [FMP], the initial binary decision variables make up the vector $\mathbf{x} \in X$ with a length of n. In order to reformulate the master problem into the QUBO formulation, we need to represent the continuous variable θ using binary bits.

$$\bar{\theta} = \sum_{i=-\underline{n}}^{\bar{n}_+} 2^i u_{i+\underline{n}} - \sum_{j=0}^{\bar{n}_-} 2^j u_{j+(1+\underline{n}+\bar{n}_+)}. \tag{22}$$

Objective Function: Because the quantum computer only accepts a quadratic polynomial over binary variables. Following the principle of the QUBO formulation, we convert the objective function to be a QUBO matrix as follows:

$$\mathbf{x_1}^\top U^\top \mathbf{x_1} + \sum_{i=-\underline{n}}^{\bar{n}_+} 2^i u_{i+\underline{n}} - \sum_{j=0}^{\bar{n}_-} 2^j u_{j+(1+\underline{n}+\bar{n}_+)} \tag{23}$$

$$= \mathbf{x_1}^\top U^\top \mathbf{x_1} + c^\top \mathbf{u}, \tag{24}$$

where $\mathbf{u}$ is the vector of binary decision variables u_i, and c is the coefficient vector. Consequently, we can merge the two binary vectors and transform (24) to

$$\begin{aligned} \mathbf{Q}_{obj} &= \mathbf{x}^\top (U + \mathrm{diag}(c))\mathbf{x} \\ &= \mathbf{x}^\top \mathbf{Q} \mathbf{x}. \end{aligned} \tag{25}$$

According to the definition, the QUBO model is unconstrained. However, constraints (19b) - (19e) need to be added to the Hamiltonian function added to QUBO model as a penalty term [27]. For example, (19b) is transformed to

$$\mathbf{H}_1 = P_1 (\sum_{z \in \mathcal{Z}} x_{i,z,t} - 1)^2, \forall i \in \mathcal{TK}, t \in \mathcal{T}, \tag{26}$$

where P_1 is the penalty weight. Only when $\sum_{z \in \mathcal{Z}} x_{i,z,t}$ equal to 1, $\mathscr{H}_1$ gets the minimum value.

For constraint (19c), the equivalent penalty is

$$\mathbf{H}_2 = P_2 (\sum_{i \in \mathcal{TK}} x_{i,z,t} - NTK_{z,t} + s_{z,t}^1)^2, \forall z \in \mathcal{Z}, t \in \mathcal{T}, \tag{27}$$

where $s_{z,t}^1$ is a slack variable, $s_{z,t}^1 \geq 0$.

Then, for constraint (19d) and (19e), according to [25], the equivalent penalty is

$$\begin{aligned} \mathbf{H}_3 =& P_3 \{ M^v \sum_{i: x_i^v = 0} x_i + M^v \sum_{i: x_i^v = 1} (1 - x_i) + \theta \\ & - d^T y^v - s_{z,t}^2 \}^2, \end{aligned} \tag{28}$$

$$\mathbf{H}_4 = P_4 \{ \sum_{i: x_i^v = 0} x_i + \sum_{i: x_i^v = 1} (1 - x_i) + \theta - 1 - s_{z,t}^3 \}^2, \tag{29}$$

while the final QUBO formulation is:

$$\mathbf{Q}_{fin} = \mathbf{Q}_{obj} + \mathbf{H}_1 + \mathbf{H}_2 + \mathbf{H}_3 + \mathbf{H}_4. \tag{30}$$

IV. Quantum Processing Unit Solver Workflow

Solving optimization problems with a QPU, involves a few critical steps using quantum annealing. First, the problem must be converted into a compatible format, either as a QUBO or Ising model. Secondly, this mathematical representation is then mapped onto the QPU's qubits through a process known as embedding, which aligns the problem variables with the QPU's qubit topology. Thirdly, before execution, parameters controlling the quantum annealing process, such as annealing time and qubit interactions, are finely tuned. The QPU then performs quantum annealing, guiding the qubits toward the lowest-energy state, which represents the problem's optimal solution. After the process, the QPU outputs the qubit states, which are translated back into the problem variables, especially if embedding was used.

In Benders' decomposition, particularly within the framework of quantum annealing, the sampling strategy is adaptive and contingent on the increasing complexity of the problem. As the decomposition progresses and the number of qubits—representing the problem's dimensionality—grows, a correspondingly larger number of samples is required to explore the solution space effectively and to increase the probability of finding the minimum energy state. The complexity of the energy landscape escalates with the addition of each qubit, enhancing the likelihood of encountering local minima.

To articulate this strategy, the following formulation is employed:

$$\text{Samples} = \alpha \cdot \text{qubits} \cdot \ln(\beta \cdot \text{iteration}), \tag{31}$$

where α and β are scaling factors. The factor α establishes the base number of samples, which is then multiplied by the current count of qubits. The logarithmic term $\ln(\beta \cdot \text{iteration})$ allows the sample size to increase in a manner that is logarithmically proportional to the number of iterations, thereby ensuring that the number of samples grows in accordance with the problem's increasing complexity.

V. Simulation and Results

The proposed approach is tested on a hybrid hydrogen and power system. The electricity part is based on IEEE 33-bus system. The hydrogen route and demand configurations are illustrated in Fig. 2, which includes three trucks, four zones, and two steam methane reformers. For testing purposes, electrolyzors and solar plants are added to the IEEE 33-bus

system. Modeling of truck-mounted mobile hydrogen storage facilities and benefits of synergistic operations of the power and hydrogen system are demonstrated in Subsection V-A with 24-hour cases. We further show how the proposed quantum assisted combinatorial Benders' decomposition algorithm outperforms the classical version in Subsection V-B with various cases under the limit of current QPU hardware.

A. Performance of Coordinated Dispatch

The cost of hydrogen production is assumed to be $640 per ton, and the efficiency of the power-to-hydrogen process is around 53%.

In this section, we design different cases to evaluate the performance of a synergistic system. The following five cases are discussed:

- Case 1: The base case is considered with a photovoltaic (PV) generation system at Bus 2, and without electrolyzer (which indicates no interactions between hydrogen and power systems), while the number of trucks is 3.
- Case 2: An electrolyzer is placed at Bus 4, which is close to the PV generation system at Bus 2, while the number of trucks is 3.
- Case 3: The electrolyzer in Case 2 is relocated from Bus 4 to Bus 16 to be far away from the PV generation system at Bus 2, while the number of trucks is 3.
- Case 2a: The electrolyzer is placed at Bus 4, while the number of trucks is 4.
- Case 3a: The parameter is similar to Case 3, while the capacity of truck is 1.5 ton.

In Tables II and IV, the dispatch results in Cases 1, 2 and 3 at Hours 6-9 are listed. For Case 1, there is no electrolyzor and the hydrogen is mainly produced by steam methane reformers in Zones 1 & 2, then transported by trucks to meet the demands in Zones 3 & 4. In Case 2, the electrolyzor is located in Bus 4, which is near the solar generation systems. Thus, the hydrogen demands are mainly supplied by solar power which is transformed to electricity by solar generation and then transformed to hydrogen by electrolyzor. In Case 3, the electrolyzor is far away from solar generation system. Though the solar power is sufficient, its delivery in power distribution system is limited by the capacity of transmission lines. Thus, the steam methane reformers and electrolyzor work simultaneously to produce hydrogen. The parameters of Case 3a are similar to Case 3 but the storage capacity of trucks is 1.5 ton. It leads to that the truck can not transport the hydrogen in time. Thus, we require SMR produce more hydrogen to satisfy the demand.

The dispatch results in Cases 1, 2, and 3 at Hours 11–14 are listed in Table III. We notice that in Case 2, even when there is no solar generation, eletrolyzor can also buy electricity from the wholesale market when the electricity price is lower than the hydrogen generation cost. From Fig. 4 we have the dispatchability of solar generation. The blue columns represent the available solar power. In Case 1, solar power can only be used in the power distribution system. Thus, the power utilization level is low, and most solar energy is wasted. In Case 2, the eletrolyzor transforms electricity to hydrogen and

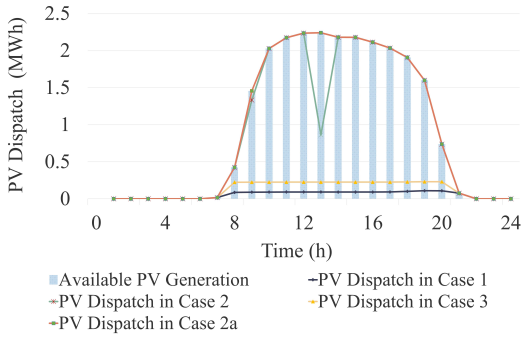

Fig. 4. Comparison of the dispatched solar power in cases with forecasted solar power generation

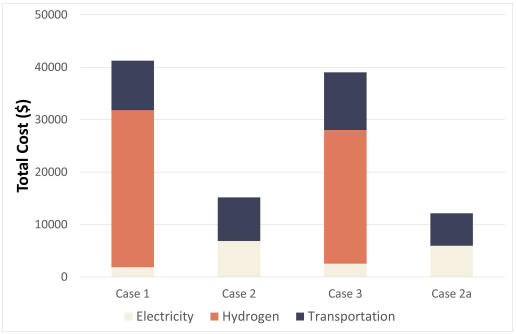

Fig. 5. Cost comparison of the four cases

stores it in truck tanks in zones when the solar power is sufficient. Thus, the power is fully utilized from Hours 7-10. However, the power transformation is also limited by the storage level and in zones. When the tank in the connected zone is full and the trucks cannot transport the extra hydrogen in time, the electrolyzor cannot transport hydrogen to the hydrogen system. Thus, the power utilization level drops in 11-14 hours. In Case 3, the utilization level is higher than in Case 1 but limited by the capacity of transmission lines. Thus, the electrolyzor should be relocated to the bus which is close to the renewable power generation unit to improve the utilization level.

The proposed synergistic operation approach enhances the dispatchability of solar power generation, as shown in Fig. 4. Compared to Case 1, the total curtailment reduces dramatically in Case 2. This is because the electrolyzor can transform the extra solar energy into hydrogen and store it in the storage. The utilization level drops during time periods 11 to 14 because the truck storage is full and reaches the maximum ability of transportation. Compared to Case 2, the total curtailment also reduces in Case 2a. Because we have more mobile trucks to store hydrogen. Thus, the utilization level is limited by the mobile truck capacity.

Fig. 6 illustrates how the coordinated system improves solar power utilization across different scenarios by balancing the availability of solar power and the proximity of the solar station to the hydrogen electrolyzor.

In Fig. 6a, where the solar power is sufficient, and the

TABLE I
TRUCK ROUTE RESULTS FOR HOURS 2-10

	2	3	4	5	6	7	8	9	10
T1	Z1: -1.35	Z3: +1.35	Z2:0	Z2:-0.15	Z3:0	Z3:+0.15	Z2:-0.3	Z1:-1.48	Z3:+1.78
T2	Z2:0	Z2:0	Z2:-0.81	Z1:0	Z1:-1.18	Z3:0	Z3:0	Z3:+2	Z2:-2
T3	Z2: -2	Z2:0	Z3:0	Z3:0	Z3:+2	Z2:-2	Z3:+2	Z1:-2	Z3:+1.35

* Zx:y means loading y ton hydrogen from zone number x (i.e., Zx)

TABLE II
DISPATCH RESULTS FOR HOURS 6-9

Cases	Time	Truck Storage (ton)			Hydrogen Production (ton)		
		T1	T2	T3	HE	HR1	HR2
Case 1	6	1.22	2	1.09	/	1	1
	7	0.51	2	1.09	/	1	0.49
	8	2	2	0	/	1	1
	9	2	1.26	2	/	1	0
Case 2	6	1.84	0	2	0	/	/
	7	2	0	0	0	/	/
	8	1.69	0	2	0.26	/	/
	9	0.21	2	0	1.12	/	/
Case 3	6	2	2	0.27	0.064	1	0
	7	2	2	0.27	0.064	1	0
	8	2	2	2	0.077	0.46	1
	9	0.15	1.2	0	0.076	0	1

TABLE III
DISPATCH RESULTS FOR HOURS 11-14

Cases	Time	Truck Storage (ton)			Hydrogen Production (ton)		
		T1	T2	T3	HE	HR1	HR2
Case 1	11	2	0	0.69	/	1	1
	12	2	1.3	2	/	1	1
	13	0	0	0	/	0	1
	14	0	2	2	/	0.3	1
Case 2	11	2	0	2	1.405	/	/
	12	2	2	0	1.06	/	/
	13	0	0	2	1.06	/	/
	14	0	2	2	1.06	/	/
Case 3	11	0	0	0	0.075	1	1
	12	2	0	0	0.075	0.72	1
	13	0	0	2	0.075	0	1
	14	0	2	0	0.075	0.57	1

TABLE IV
DISPATCH RESULTS FOR DIFFERENT TRUCK CAPACITY

Cases	Time	Truck Storage (ton)			Hydrogen Production (ton)		
		T1	T2	T3	HE	HR1	HR2
Case 3	6	2	2	0.27	0.064	1	0
	7	2	2	0.27	0.064	1	0
	8	2	2	2	0.077	0.46	1
	9	0.15	1.2	0	0.076	0	1
Case 3a	6	1.5	1.5	1.23	0.064	1	0
	7	1.5	1.5	0.27	0.064	1	0
	8	1.5	1.5	1.5	0.077	0.82	1
	9	0.34	1.4	0	0.076	0	1

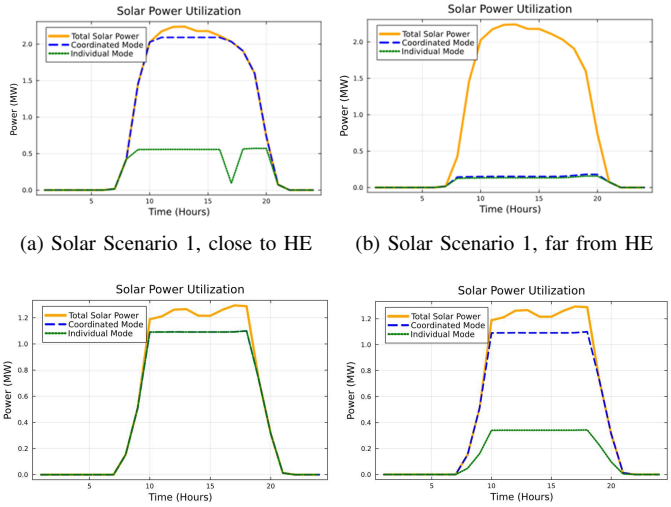

(a) Solar Scenario 1, close to HE (b) Solar Scenario 1, far from HE

(c) Solar Scenario 2, far from HE (d) Solar Scenario 2, close to HE

Fig. 6. Comparisons of Scenarios with Different Renewable Power Utilization Level

solar station is located near the hydrogen electrolyzor, both the electricity system and the hydrogen production system can make full use of the available solar power. This allows the hydrogen system to benefit from the solar energy to produce hydrogen, as shown by the effective utilization in the coordinated mode. The close proximity allows efficient energy transfer, reducing losses and ensuring that both systems optimize the renewable energy resource.

In Fig. 6b, despite having sufficient solar power, the solar station is located far from the hydrogen electrolyzor. This geographical distance limits the utilization of solar power, primarily because of the constraints of the electricity transmission lines. The transmission capacity is insufficient to transport the full amount of available solar energy, leading to a reduction in the overall utilization of solar power by the hydrogen system. As a result, the solar energy that can be directed to the hydrogen electrolyzor is limited, reflecting suboptimal use of the resource.

In Fig. 6c, the solar power availability is limited, but the electricity system is capable of fully utilizing what is available. However, the hydrogen production system is unable to access renewable solar power due to the limited supply. The coordinated system ensures that the available solar power is directed to meet the electricity demand first, leaving the hydrogen system without renewable power, which signifies that the prioritization of energy use is towards electricity consumption.

In Fig. 6d, the solar station is again located near the hydrogen electrolyzor. Although the total solar power is not as abundant, the proximity to the electrolyzor allows the hydrogen system to effectively tap into the renewable energy source. This leads to an improvement in the hydrogen system's ability to utilize the available solar power. The coordinated mode ensures that the solar power is used efficiently, with a focus on supplying the electrolyzor, demonstrating how geographical proximity and system coordination can maximize renewable energy usage for hydrogen production.

This analysis highlights how the coordinated system dynamically adjusts based on the spatial and resource conditions, optimizing solar power utilization and ensuring effective energy use across electricity and hydrogen systems.

We use 4 different cases to evaluate the performance of our synergistic model, while the performance is shown in Fig. 5. In Case 1, there is no electrolyzor and the power and hydrogen system is independent. For Case 2, there is a electrolyzor close to the solar generation system. In Case 2, our proposed synergistic model save 66% money from \$41,229 to \$15,183, as the electrolyzor can fully utilize the renewable power from the solar generation system. Especially, the hydrogen generation cost in Case 1 is \$14,906 and in Case 2 it is zero. In Case 3, the total cost is \$39,973, lower than Case 1 but much higher than Case 2. Because the electrolyzor is far from solar generation system and the utilization level of renewable power is low.

The performance of Case 2a is shown in Figs. 4 and 5 to evaluate the performance of different number of trucks in the coordinate system. The Case 2a has the same parameters of Case 2 except the number of trucks is 4 rather than 3. From Case 2, we notice that at time periods 11 to 14 there is a sharp decrease of renewable power utilization level. Because all trucks are on their way and cannot transport the transformed hydrogen to other zones in time. However, in Case 2a we have sufficient trucks and can fully utilize the renewable power from solar generator unit. Fig. 5 also shows that more trucks can decrease the hydrogen production cost. The routine of 3 trucks are listed in Table I, our model select the transportation routine which achieves the minimum fuel cost.

B. Performance of Quantum Assisted Combinatorial Benders' Decomposition

We tested cases with different sizes to compare the performance of our quantum-assisted combinatorial Benders' decomposition algorithms with a classical version whose master problems are solved by commercial solvers on conventional computers. The experiments were conducted using the Gurobi solver and the D-Wave annealer. The result of the master problem is shown in Fig. 7. We notice that with the increase of Benders' cuts, the time consumption of the classical solver in each round increases exponentially because more constraints are added. What is more, the nonlinear problem is difficult for classical solvers to solve. However, the time consumption of quantum annealer at each iteration for the master problem remains relatively stable because as the complexity of quantum annealing mainly depends on the number of qubits.

Figs. 7 (d), (e), and (f) show the cumulative time comparisons of difference methods for master problem-solving. Although the classical solver (labeled as 'Gurobi') requires less time compared to the quantum solver (labeled as 'QPU') in a smaller-sized problem in (b), our algorithm shows a trend to outperform the classical version as the problem scale increases in Figs. 7 (e) and (f). The classical solver's time requirement appears to grow at an exponential rate with the problem size increases, reflecting the expected computational complexity for larger instances. In contrast, the quantum solver's curve shows a milder increase. This indicates that the quantum solver, leveraging the principles of quantum mechanics, scales better with problem size and thus can save more time as problems become more complex. It suggests a potential computational advantage of quantum solvers over classical ones in dealing with large-scale optimization problems, where classical methods become impractical due to their steep rise in time complexity. This indicates that the QPU solver scales better with problem size and suggests that for sufficiently large and complex problem instances, the QPU solver may become the more time-efficient option compared to Gurobi.

Overall, the quantum assisted combinatorial Benders' decomposition algorithm and quantum annealer have advantages when the size of the optimization problem becomes larger.

VI. Conclusion

To improve the operation efficiency of hydrogen and power distributed systems, this paper proposed a synergistic dispatch approach, which leverages the flexibility from the hydrogen system to accommodate renewable energy fluctuations. Our simulation results demonstrated that, with the ability of energy conversion, the synergistic dispatch could reduce over 66% system cost in the specific test system. The efficiency of renewable power utilization is also improved. Our simulation results also demonstrated the computational efficiency of the proposed Benders' decomposition on hybrid quantum and classical computers.

References

[1] C. Xu, K. Wang, P. Li, R. Xia, S. Guo, and M. Guo, "Renewable energy-aware big data analytics in geo-distributed data centers with reinforcement learning," *IEEE Transactions on Network Science and Engineering*, vol. 7, no. 1, pp. 205–215, Mar. 2020.

[2] W. Xiao, Y. Cheng, W.-J. Lee, V. Chen, and S. Charoensri, "Hydrogen filling station design for fuel cell vehicles," *IEEE Transactions on Industry Applications*, vol. 47, no. 1, pp. 245–251, Nov. 2011.

[3] R. Dufo-López, J. L. Bernal-Agustín, and J. Contreras, "Optimization of control strategies for stand-alone renewable energy systems with hydrogen storage," *Renewable Energy*, vol. 32, no. 7, pp. 1102–1126, Jun. 2007.

[4] Z. Shen, C. Wu, L. Wang, and G. Zhang, "Real-time energy management for microgrid with EV station and CHP generation," *IEEE Transactions on Network Science and Engineering*, vol. 8, no. 2, pp. 1492–1501, Mar. 2021.

[5] S. Nojavan, K. Zare, and B. Mohammadi-Ivatloo, "Application of fuel cell and electrolyzer as hydrogen energy storage system in energy management of electricity energy retailer in the presence of the renewable energy sources and plug-in electric vehicles," *Energy Conversion and Management*, vol. 136, pp. 404–417, Mar. 2017.

[6] M. Chen, Z. Shen, L. Wang, and G. Zhang, "Intelligent energy scheduling in renewable integrated microgrid with bidirectional electricity-to-hydrogen conversion," *IEEE Transactions on Network Science and Engineering*, vol. 9, no. 4, pp. 2212–2223, Mar. 2022.

[7] X. Cao, X. Sun, Z. Xu, B. Zeng, and X. Guan, "Hydrogen-based networked microgrids planning through two-stage stochastic programming with mixed-integer conic recourse," *IEEE Transactions on Automation Science and Engineering*, vol. 19, no. 4, pp. 3672–3685, Oct. 2021.

[8] J. Liu, Z. Xu, J. Wu, K. Liu, X. Sun, and X. Guan, "Optimal planning of internet data centers decarbonized by hydrogen-water-based energy systems," in *IEEE 17th International Conference on Automation Science and Engineering (CASE)*, Lyon, France, Aug. 2021, pp. 1276–1281.

[9] S. Wang and R. Bo, "Joint planning of electricity transmission and hydrogen transportation networks," *IEEE Transactions on Industry Applications*, vol. 58, no. 2, pp. 2887–2897, Mar.-Apr. 2022.

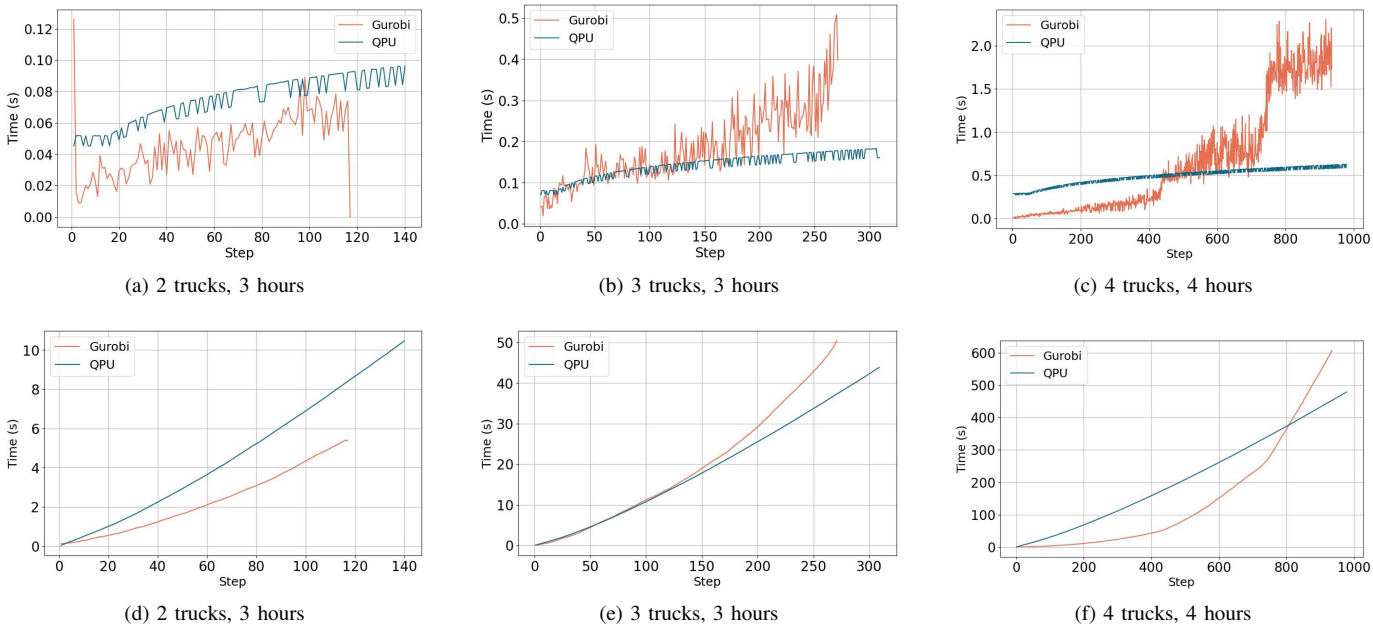

(a) 2 trucks, 3 hours (b) 3 trucks, 3 hours (c) 4 trucks, 4 hours

(d) 2 trucks, 3 hours (e) 3 trucks, 3 hours (f) 4 trucks, 4 hours

Fig. 7. Comparisons of classical and quantum-assist Benders' Decomposition: (a), (b) and (c) represent master problem solution time in each iteration, with increased problem size; (d), (e) and (f) are accumulated time respectively.

[10] H. Gómez-Villarreal, M. Cañas-Carretón, R. Zárate-Miñano, and M. Carrión, "Generation capacity expansion considering hydrogen power plants and energy storage systems," *IEEE Access*, vol. 11, pp. 15 525–15 539, Feb. 2023.

[11] J. Li, J. Lin, Y. Song, X. Xing, and C. Fu, "Operation optimization of power to hydrogen and heat (P2HH) in ADN coordinated with the district heating network," *IEEE Transactions on Sustainable Energy*, vol. 10, no. 4, pp. 1672–1683, Sep. 2019.

[12] H. Khani, N. A. El-Taweel, and H. E. Z. Farag, "Supervisory scheduling of storage-based hydrogen fueling stations for transportation sector and distributed operating reserve in electricity markets," *IEEE Transactions on Industrial Informatics*, vol. 16, no. 3, pp. 1529–1538, 2020.

[13] M. Zare Oskouei, H. Mehrjerdi, and P. Palensky, "Risk-constrained bidding and offering strategy for sector-coupled electricity-hydrogen systems incorporating accessibility level of mobility sector," *Journal of Cleaner Production*, vol. 451, p. 142031, 2024.

[14] M. Li, S. Wang, L. Fan, and Z. Han, "Coordinated operations of hydrogen and power distribution systems," in *IEEE PES Innovative Smart Grid Technologies Conference (ISGT)*, Washington, DC, Feb. 2023.

[15] A. M. Geoffrion, "Generalized Benders' Decomposition," *Journal of Optimization Theory and Applications*, vol. 10, no. 4, pp. 237–260, Oct. 1972.

[16] A. Giani and Z. Eldredge, "Quantum computing opportunities in renewable energy," *SN Computer Science*, vol. 2, no. 3, p. 393, Mar. 2021.

[17] A. Ajagekar and F. You, "Quantum computing and quantum artificial intelligence for renewable and sustainable energy: A emerging prospect towards climate neutrality," *Renewable and Sustainable Energy Reviews*, vol. 165, p. 112493, Sep. 2022.

[18] National Academies of Sciences, Engineering, and Medicine and others, *Quantum computing: progress and prospects*. Washington, DC: National Academies Press, 2019.

[19] R. Li, Y. He, S. Zhang, J. Qin, and J. Wang, "Cell membrane-based nanoparticles: a new biomimetic platform for tumor diagnosis and treatment," *Acta Pharmaceutica Sinica B*, vol. 8, no. 1, pp. 14–22, Jan. 2018.

[20] E. Grant, T. S. Humble, and B. Stump, "Benchmarking quantum annealing controls with portfolio optimization," *Physical Review Applied*, vol. 15, no. 1, p. 014046, Jan. 2021.

[21] S. Harwood, C. Gambella, D. Trenev, A. Simonetto, D. Bernal, and D. Greenberg, "Formulating and solving routing problems on quantum computers," *IEEE Transactions on Quantum Engineering*, vol. 2, pp. 1–17, Jan. 2021.

[22] L. Fan and Z. Han, "Hybrid quantum-classical computing for future network optimization," *IEEE Network*, vol. 36, no. 5, pp. 72–76, Nov. 2022.

[23] N. G. Paterakis, "Hybrid quantum-classical multi-cut Benders approach with a power system application," *Computers & Chemical Engineering*, vol. 172, p. 108161, Apr. 2023.

[24] J. Naoum-Sawaya and S. Elhedhli, "A nested Benders decomposition approach for telecommunication network planning," *Naval Research Logistics (NRL)*, vol. 57, no. 6, pp. 519–539, Jul. 2010.

[25] Z. Zhao, L. Fan, and Z. Han, "Hybrid quantum Benders' Decomposition for mixed-integer linear programming," in *IEEE Wireless Communications and Networking Conference (WCNC)*, Austin, TX, Apr. 2022, pp. 2536–2540.

[26] R. Nembrini, M. Ferrari Dacrema, and P. Cremonesi, "Feature selection for recommender systems with quantum computing," *Entropy*, vol. 23, no. 8, p. 970, Jul. 2021.

[27] F. Glover, G. A. Kochenberger, R. Hennig *et al.*, "Quantum bridge analytics I: a tutorial on formulating and using QUBO models," *Annals of Operations Research*, vol. 314, pp. 141–183, Nov. 2022.

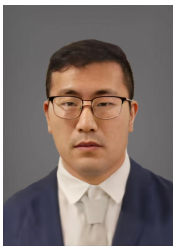

Mingze Li (Student Member, IEEE) He received his B.S. degree in Electrical Engineering from Tianjin University, China, in 2017, and a Master's degree in Computer Engineering from San Jose State University, CA, USA, in 2020. He is currently a Ph.D. candidate at the University of Houston. His research interests include the optimization of hydrogen systems, quantum optimization, and electricity power network.

Siyuan Wang (Senior Member, IEEE) received the B.S. and Ph.D. degrees in electrical engineering from Zhejiang University. He is currently an Energy Systems Engineer in the Energy Systems and Infrastructure Analysis Division, Argonne National Laboratory.

Lei Fan (Senior Member, IEEE) is an Assistant Professor with the department of Engineering Technology and the department of Electrical and Computer Engineering at the University of Houston. Before this position, he worked in the power industry for several years. He received the Ph.D. degree in operations research from the Industrial and System Engineering Department at the University of Florida. His research includes quantum computing, optimization methods, complex system operations, power system operations, and planning.

Zhu Han (Fellow, IEEE) received the B.S. degree in electronic engineering from Tsinghua University, in 1997, and the M.S. and Ph.D. degrees in electrical and computer engineering from the University of Maryland, College Park, in 1999 and 2003, respectively.

From 2000 to 2002, he was an R&D Engineer of JDSU, Germantown, Maryland. From 2003 to 2006, he was a Research Associate at the University of Maryland. From 2006 to 2008, he was an assistant professor at Boise State University, Idaho. Currently, he is a John and Rebecca Moores Professor in the Electrical and Computer Engineering Department as well as in the Computer Science Department at the University of Houston, Texas. Dr. Han's main research targets on the novel game-theory related concepts critical to enabling efficient and distributive use of wireless networks with limited resources. His other research interests include wireless resource allocation and management, wireless communications and networking, quantum computing, data science, smart grid, carbon neutralization, security and privacy. Dr. Han received an NSF Career Award in 2010, the Fred W. Ellersick Prize of the IEEE Communication Society in 2011, the EURASIP Best Paper Award for the Journal on Advances in Signal Processing in 2015, IEEE Leonard G. Abraham Prize in the field of Communications Systems (best paper award in IEEE JSAC) in 2016, IEEE Vehicular Technology Society 2022 Best Land Transportation Paper Award, and several best paper awards in IEEE conferences. Dr. Han was an IEEE Communications Society Distinguished Lecturer from 2015 to 2018 and ACM Distinguished Speaker from 2022 to 2025, AAAS fellow since 2019, and ACM Fellow since 2024. Dr. Han is a 1% highly cited researcher since 2017 according to Web of Science. Dr. Han is also the winner of the 2021 IEEE Kiyo Tomiyasu Award (an IEEE Field Award), for outstanding early to mid-career contributions to technologies holding the promise of innovative applications, with the following citation: "for contributions to game theory and distributed management of autonomous communication networks."